energies

MDPI

Article

A Step-by-Step Design for Low-Pass Input Filter of the Single-Stage Converter

Qingqing He [1,*], Lei Liu [1], Mingyang Qiu [1] and Quanming Luo [2]

[1] The School of Automation, Wuhan University of Technology, Wuhan 430070, China; liulei001@whut.edu.cn (L.L.); qiu3500@whut.edu.cn (M.Q.)
[2] State Key Laboratory of Power Transmission Equipment & System Security and New Technology, Chongqing University, Chongqing 400044, China; lqm394@126.com
* Correspondence: heqingqing@whut.edu.cn

Abstract: Active power factor correction converters are often introduced as the front stage of power electronic equipment to improve the power factor and eliminate higher harmonics. A Boost or Buck-Boost converter operating in discontinuous current mode is always adopted to achieve high power factor correction. In addition, the input current contains a large amount of higher harmonics, and a low-pass input filter is commonly adopted to filter it out. In this paper, a single-stage high-frequency AC/AC converter is taken as an example to demonstrate the design method of a passive low-pass filter. Firstly, the input side of the grid needs to meet the power factor and harmonic requirements. The preset parameters are set to a range to characterize the performance of the LC filter. The quantitative design method of input filter is proposed and summarized. Moreover, the sensitivity of the filter parameters is analyzed, providing a direction in practical applications. Preset parameters are all proved to conform to the preset range through PSIM simulation. Finally, a 130-W prototype is established to verify the correction of proposed design method. The power factor is around 0.935 and harmonic content in the input current is about 26.4%. All requirements can be satisfied.

Keywords: single-stage converter; low-pass input filter; AC/AC; parameter design

Citation: He, Q.; Liu, L.; Qiu, M.; Luo, Q. A Step-by-Step Design for Low-Pass Input Filter of the Single-Stage Converter. *Energies* **2021**, *14*, 7901. https://doi.org/10.3390/en14237901

Academic Editor: Nicu Bizon

Received: 23 October 2021
Accepted: 19 November 2021
Published: 25 November 2021

1. Introduction

In traditional electrical equipment, uncontrolled diode rectifiers or thyristor phase-controlled rectifiers with a large capacitor are often used to produce DC voltage [1,2]. Due to the nonlinearity of diodes and thyristors, the AC input current contains a large amount of harmonics, resulting in high total harmonic distortion (THD) and low input power factor (PF). The high harmonic currents might cause device malfunction, cause power substation overheating, interfere with the electrical devices nearby [3,4], etc. This prompted the establishment of power quality standards for household product emission limits (e.g., IEC555.2, IEC 61000-3-2, etc.) [5]. Active power factor correction (APFC) is widely used in modern electrical equipment, because it can reduce the THD of the input current and increase the power factor [6–8].

In small–medium power applications, single-stage converters (SSCs) are popularly used for APFC due to their simple circuit and low cost [9–12]. Figure 1 gives three typical types of single-stage converters based on the power factor correction (PFC) unit. Figure 1a shows the typical single-stage AC/DC converter-based PFC unit [13]. Figure 1b,c show the single-stage AC/DC converter based on the PFC unit with cascaded DC/DC and DC/AC unit, respectively [14,15], where the DC/DC and DC/AC unit are adopted to regulate the output voltage.

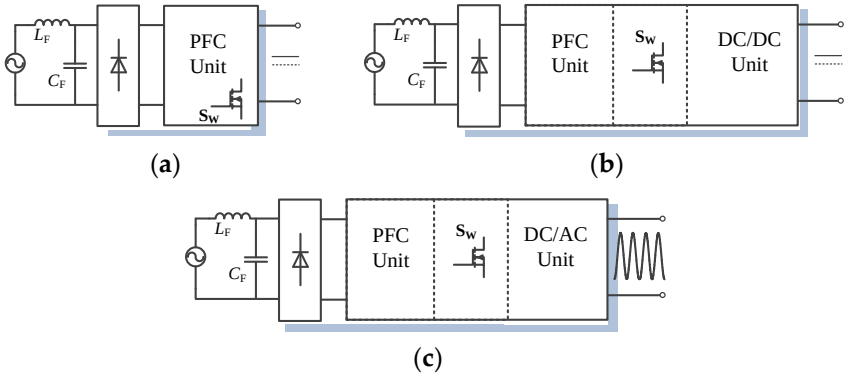

Figure 1. Structures of the SSC with APFC function. (**a**) Typical single-stage AC/DC converter. (**b**) Integrated single-stage AC/DC converter. (**c**) Integrated single-stage AC/AC converter.

For the PFC unit, a Boost or Buck-Boost converter operating in discontinuous current mode (DCM) is often adopted to achieve high PF inherently in conditions where the duty cycle of the switch remains nearly constant [16,17]. In addition, the input filter is introduced to further reduce the higher harmonics in the input current, and thus the THD requirements can be satisfied. Due to the similarities in the analysis of single-stage converters, the integrated single-stage AC/AC converter demonstrate in Figure 1c is taken as an example to study the design method of the input filter. Certainly, the method proposed in the paper is also applicable for other structures of the SSC, such as single-stage AC/DC converters [18–20].

As shown in Figure 2, the single-stage high-frequency AC/AC converter [21] is used to transform the line voltage into high-frequency AC sinusoidal output voltage, and its amplitude is constant. Then the AC output voltage can be employed to drive a high-brightness light-emitting diode (HB-LED) through a passive high-frequency AC/DC converter with a constant current [22]. As mentioned above, the PFC unit employs a Boost converter operating in DCM to convert AC power into DC power, and a high power factor can be achieved at the AC input [23–25]. The DC/AC unit uses an LC-LC series–parallel resonant inverter in zero voltage switching (ZVS) mode to provide the constant AC sinusoidal output voltage whose THD is low, and zero voltage switching (ZVS) of all the power switches can be achieved [26–28]. A voltage feedback controller is needed for the converter to regulate the amplitude of the high-frequency AC output voltage.

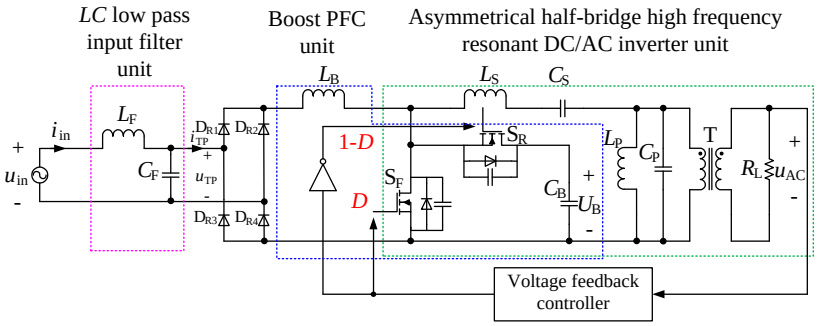

Figure 2. Single−stage high−frequency AC/AC converter with LC filter.

Since the above Boost PFC unit works in DCM, the input current contains massive switching frequency ripple. In addition, the input filter is generally adopted to eliminate these ripples so as to reduce harmonic pollution. The input filter could be either an active filter or a passive filter [29,30]. Due to the simplicity and low cost of the passive filters, they are widely used in practical applications, such as LCL filter, LC filter, series damped filter, parallel damped filter, coupled-inductor filter and so on [31–33].

There are some references about input filters [33–37], which are summarized in Table 1. The DC input filter design for DC/DC and DC/AC converter can be found in [33,34]. The minimum-component filter has been analyzed in [33]. According to the analysis of different filter forms and their transfer function, ref. [33] gives the direction on how to design and adjust inductors and capacitors, but it is not a quantitative design. The DC bus filter in [34] is composed of a bulk capacitor, high frequency capacitor and LC DC input filter. However, ref. [34] focuses on the design of bulk capacitor without the LC input filter design. There are also some AC input filters [35–37]. A LCL filter design procedure with try and error method is proposed in [35]. The capacitor design is complicated because the initial values of the current ripple, and the converter-side inductor design are not mentioned. Ref. [36] proposed an iterative process to design the L and LCL filter parameters based on the analytical expression of the voltage harmonics. In addition, an LC filter design procedure for three-phase current source rectifier is proposed in [37], which demands an estimation of the ripple component shown in the input line currents.

Table 1. Different filter design reviews.

Ref.	Filter Type		Application	Quantitative Design
[33]	DC Input filter	LC	DC/DC converter	No
[34]	DC Bus filter	C + LC	DC/AC stage of the AC/AC converter	No
[35]	AC Input filter	LCL	Three-phase active rectifier	No
[36]	AC Input filter	L/LCL	Three-phase active rectifier	Yes
[37]	AC Input filter	LC	Three-phase current source rectifier	Yes
Proposed	AC Input filter	LC	Single-phase single-stage converter	Yes

To date, there are few studies referring to quantitative parameter design of the input filter for single-phase single-stage converters; the practical approach is to determine the parameters by making simulation trial and error correction, which seems to be time-consuming and of low efficiency. In this paper, the low-pass LC filter is chosen as the input filter of the PFC unit. Its design procedure is presented step by step. Please note that the proposed design method can also be applied to other types of input filters.

The main contributions of the work mainly include the following aspects: (1) A programmatic step-by-step design method for the LC input filter of single-stage converter is proposed in the paper, which offers an easy-to-use tool. (2) The precise design method is based on the restrictions of the input harmonic currents, so an accurate analytical design procedure is presented. The proposed method can also be applied to the design of other types of input filters. (3) The sensitivity analysis provides a method that can adjust input filter parameters to the expected value accurately, which is of great value in practical applications.

The remaining part of the paper is organized as follows: in Section 2, the circuit of the LC filter is analyzed in detail; in Section 3, a detailed step-by-step programmatic design of the filter is presented in terms of three input current conditions; the sensitivity analysis of the filter is presented in Section 4; and then simulation waveforms and key experimental results are given in Sections 5 and 6, respectively; the conclusions are drawn in Section 7. Moreover, the symbols used in the design process are listed in Appendix A. The implementation design process of the inductor is shown in Appendix B. The derivations of several equations are added to Appendix C.

2. Circuit Analysis

Before the design of the input filter, necessary preparation work should be performed. Firstly, the known parameters and the preset parameters of the input filter are discussed. Since the LC filter is mainly to eliminate harmonic currents at multiples of the switching frequency, the root mean square (RMS) of the switching frequency harmonic current in the

input current before filtering is analytically derived in this section. The above work lays the foundation for the design of filter parameters. Before that, the equivalent circuit of SSC should be presented and analyzed. The specific analysis is as follows.

2.1. Known and Preset Parameters of the Input Filter

Some reasonable assumptions are made as follows before the design of the filter.

(1) No harmonics are contained in the input voltage.
(2) The energy-stored capacitor C_B is large enough so that its voltage ripple can be ignored and hence the duty cycle D of the switch S_F is assumed to remain constant during half line cycle.
(3) The input power of the converter P_{in} is equal to the output power P, which means the efficiency of the converter is supposed to be 100%, that is, η = 100%. In practical applications, the efficiency is less than 100%. Then it only needs to add corresponding coefficients between input and output for analysis, that is, $P_{in} = P/\eta$.
(4) Because of the pulse-width modulation, the dominant harmonic components of the input current occur at or around the switching frequency and its multiples. The former is the main component. Hence, assume that all the energy in the input current spectrum is concentrated on the switching frequency.

For the design of the input filter, these values should be preset in advance: the input voltage u_{in}, the converter power P, the Boost inductance L_B and the switching frequency f_{SW}. In addition, the precise design method is based on the restrictions of the input harmonic currents. Therefore, according to the operation principle of SSC, the following parameters need to be preset:

(1) m is the ratio of the fundamental component amplitude U_{TPFm} of the voltage across the AC side of the rectifier bridge to the voltage U_B across the stored-energy capacitor C_B. In addition, m must be slightly smaller than 0.9. One reason is that, considering the Boost-type PFC operating in DCM, the input power factor of the rectifier bridge can be ensured larger than 0.9 on condition that m is smaller than 0.9 [38]. Another reason is that a smaller m means a larger U_B; m = 0.8 is chosen for comprehensive consideration.
(2) The input fundamental power factor λ_F: to minimize the influence on the input power factor of the input filter, the phase angle must be small at fundamental frequency, so λ_F should be close to 1. Here, λ_F can be taken as $0.99 \leq \lambda_F \leq 1$.
(3) α is the ratio of the RMS value U_{TPF} of the voltage drop u_{TP} in fundamental component to the RMS value U_{in} of the input voltage u_{in}. Additionally, α must be close to unity so that the voltage drop in the fundamental component across the filter is small, and an enhanced efficiency can be obtained as well as power density. Therefore, α can be taken as $0.98 \leq \alpha \leq 1.02$.
(4) For the voltage drop u_{TP} across the AC side of the rectifier bridge, β is the ratio of the RMS value U_{TPSW} of the harmonic component at the switching frequency to the RMS value U_{TPF} of the component at the grid frequency. In addition, β should be set within a small limit so that the input voltage of SSC has a limited amount of high harmonic ripple U_{TPSW} to ensure the proper operation of the SSC. Therefore, β can be taken as $0.0005 \leq \beta \leq 0.005$.
(5) For the input current, γ is the ratio of the RMS value I_{TPSW} of the harmonic component at the switching frequency to the RMS value I_{TPF} of the fundamental component at grid frequency. It should be set within a small limit to reduce the harmonic current at the switching frequency. Therefore, γ can be taken as $0.0001 \leq \gamma \leq 0.001$.

The interaction between the LC filter and the single-stage AC/AC converter involves the above parameters. Based on the above assumptions, and known and preset parameters, a passive LC filter is taken as an example to demonstrate the parameter design of the input filter for SSC in the next section.

2.2. Equivalent Circuit of SSC

This section is preparation for the filter design. The equivalent circuit of the SSC is firstly derived and analyzed according to its operating principle and performance properties. Then the RMS of the harmonic current at the switching frequency on the AC side of the rectifier bridge is computed.

Figure 3 gives an equivalent circuit of SSC based on the PFC circuit, where the DC/DC unit or DC/AC unit in the SSC is replaced by an equivalent resistor R_B when operating in steady state.

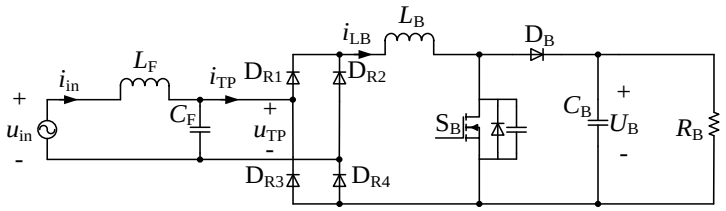

Figure 3. Equivalent circuit of the SSC with LC filter.

In the above PFC circuit, the Boost inductor L_B is designed for operation in the discontinuous current mode (DCM) with a fixed duty cycle. The duty cycle D is almost constant. Also, the inductor current i_{LB} is discontinuous within an AC line cycle, so the envelope of input current is a sine waveform in phase with the AC line input voltage u_{in}. Then high input power factor can be achieved inherently. The driving signal of switches Q_{SF} and Q_{SR}, input voltage u_{in} and input current i_{TP} are shown in Figure 4.

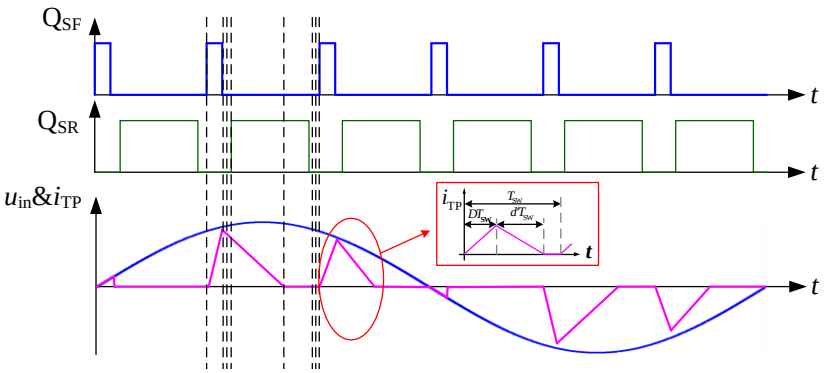

Figure 4. The operation waveforms of the PFC unit in steady state.

According to the above mentioned known and preset parameters, u_{TP} is almost equal to u_{in}, the following can be obtained

$$u_{TP} \approx u_{in} = U_{inm} \sin \omega t = \sqrt{2} U_{in} \sin \omega t \tag{1}$$

Additionally, according to the definition of m, the following can be obtained

$$U_B = \frac{U_{TPFm}}{m} \approx \frac{U_{inm}}{m} \tag{2}$$

The output power of SSC is expressed as

$$P = \frac{{U_B}^2}{R_B} \tag{3}$$

Then, R_B can be derived from the following equation

$$R_{\mathrm{B}} = \frac{{U_{\mathrm{inm}}}^2}{m^2 P} \tag{4}$$

Since the Boost PFC unit is operating in DCM, the waveform of current i_{TP} on the AC line side of the rectifier bridge and its waveform over one switching cycle T_{SW} is drawn in Figure 4. Equation (5) is obtained by averaging i_{TP} over one switching cycle.

$$\bar{i}_{\mathrm{TP}} = \frac{D^2 T_{\mathrm{SW}} U_{\mathrm{inm}}}{2L_{\mathrm{B}}} \frac{\sin \omega t}{1 - m|\sin \omega t|} \tag{5}$$

From (5), the RMS of i_{TP} at the fundamental frequency can be obtained as follows

$$I_{\mathrm{TPF}} = \frac{D^2 T_{\mathrm{SW}} U_{\mathrm{in}} A}{L_{\mathrm{B}}} \tag{6}$$

where

$$A = \frac{1}{\pi} \int_0^{\pi} \frac{\sin^2 \omega t}{1 - m \sin \omega t} d(\omega t) \tag{7}$$

Approximately, the power of SSC can also be expressed as

$$P = \frac{U_{\mathrm{TPFm}} I_{\mathrm{TPFm}}}{2} \approx \frac{U_{\mathrm{inm}} I_{\mathrm{TPFm}}}{2} = U_{\mathrm{in}} I_{\mathrm{TPF}} \tag{8}$$

From the above equations, the duty cycle D of the switch $\mathrm{S_B}$ in the following can be obtained as

$$D = \sqrt{\frac{P L_{\mathrm{B}}}{{U_{\mathrm{in}}}^2 A T_{\mathrm{SW}}}} \tag{9}$$

From (9), the duty cycle D is determined, since U_{in}, P, L_{B}, and T_{SW} are all known, and i_{TP} can also be determined. According to the principle of equivalence, SSC can be replaced by a current source. Therefore, the AC side equivalent circuit of SSC can be obtained as shown in Figure 5a. Base on the previous assumptions, the current source contains not only the fundamental component at the grid frequency, but also current ripples at the switching frequency. Using the principle of superposition, the two equivalent circuits when either component works alone are shown in Figures 5b and 5c, respectively.

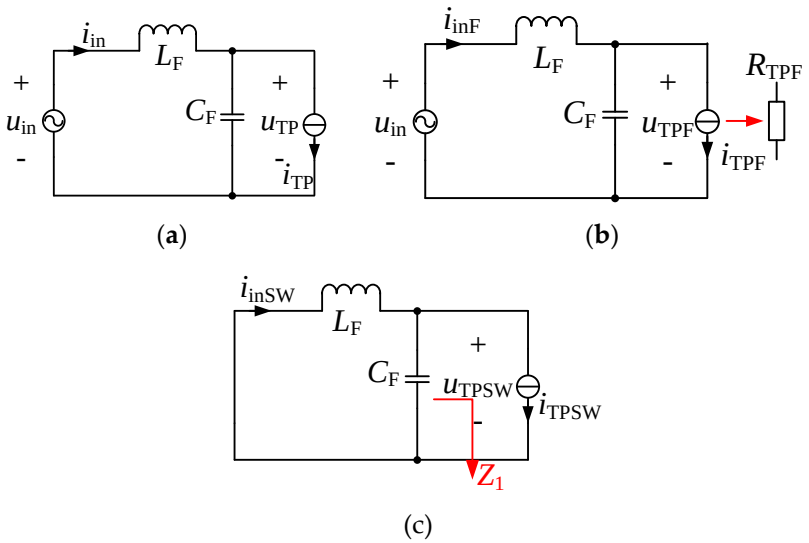

Figure 5. (**a**) AC side equivalent circuit of SSC. (**b**) The equivalent circuit when the fundamental component works alone. (**c**) The equivalent circuit when the harmonic component works alone.

Because u_{TPF} is almost in phase with i_{TPF} by appropriate modulation, the current source i_{TPF} can be replaced by an equivalent resistor R_{TPF}, whose value can be calculated as (10).

$$R_{\mathrm{TPF}} = \frac{{U_{\mathrm{in}}}^2}{P} \tag{10}$$

For Figure 5c, to obtain the RMS value of i_{inSW}, it is necessary to obtain the expression of i_{TPSW}.

2.3. The RMS Value of the Current at Switching Frequency on the AC Side of the Rectifier—I_{TPSW}

On the basis of the working principle of the Boost PFC unit, the instantaneous inductor current i_{LB} (kT_{SW}) can be expressed as (11) over the k-th switching period.

$$i_{\mathrm{LB}}(kT_{\mathrm{SW}}) = \begin{cases} \frac{u_{\mathrm{k}}}{L_{\mathrm{B}}}(t - kT_{\mathrm{SW}}), & t \in [kT_{\mathrm{SW}}, (k+D)T_{\mathrm{SW}}] \\ \frac{U_{\mathrm{B}}DT_{\mathrm{SW}} + (u_{\mathrm{k}} - U_{\mathrm{B}})[t-(k+D)T_{\mathrm{SW}}]}{L_{\mathrm{B}}}, & t \in [(k+D)T_{\mathrm{SW}}, (k+D+d'_{\mathrm{k}})T_{\mathrm{SW}}] \\ 0, & t \in [(k+D+d'_{\mathrm{k}})T_{\mathrm{SW}}, (k+1)T_{\mathrm{SW}}] \end{cases} \tag{11}$$

where

$$u_{\mathrm{k}} = \sqrt{2}U_{\mathrm{IN}}|\sin \omega k T_{\mathrm{SW}}| \tag{12}$$

In steady state, the inductance voltage-second balance is always met for Boost inductor L_{B} and the following equation can easily be obtained:

$$d'_{\mathrm{k}} = \frac{u_{\mathrm{k}}D}{U_{\mathrm{B}} - u_{\mathrm{k}}} \tag{13}$$

From (11) and (13), the expression of the square RMS value of Boost inductor current i_{LB} over one switching cycle can be obtained as

$$\begin{aligned} &\langle i_{\mathrm{LB}} \rangle^2_{\mathrm{RMS},T_{\mathrm{SW}}}(kT_{\mathrm{SW}}) \\ &= \tfrac{1}{T_{\mathrm{SW}}} \textstyle\int_{kT_{\mathrm{SW}}}^{(k+1)T_{\mathrm{SW}}} [i_{\mathrm{LB}}(kT_{\mathrm{SW}})]^2 dt \\ &= \tfrac{1}{T_{\mathrm{SW}}} \left\{ \textstyle\int_0^{DT_{\mathrm{SW}}} \left(\frac{u_{\mathrm{k}}}{L_{\mathrm{B}}}t\right)^2 dt + \int_{DT_{\mathrm{SW}}}^{(D+d'_{\mathrm{k}})T_{\mathrm{SW}}} \left[\frac{U_{\mathrm{B}}DT_{\mathrm{SW}} + (u_{\mathrm{k}} - U_{\mathrm{B}})(t - DT_{\mathrm{SW}})}{L_{\mathrm{B}}}\right]^2 dt \right\} \\ &= \tfrac{D^3}{3}\left(\tfrac{T_{\mathrm{SW}}}{L_{\mathrm{B}}}\right)^2 \tfrac{U_{\mathrm{B}} \cdot u_{\mathrm{k}}^2}{U_{\mathrm{B}} - u_{\mathrm{k}}} \end{aligned} \tag{14}$$

Based on (14), the expression of the square RMS value of Boost inductor current i_{LB} over half line cycle is as follows:

$$\begin{aligned} \langle i_{\mathrm{LB}} \rangle^2_{\mathrm{RMS},T} &= \tfrac{2}{T} \textstyle\sum_k \langle i_{\mathrm{LB}} \rangle^2_{\mathrm{RMS},T_{\mathrm{SW}}}(kT_{\mathrm{SW}})T_{\mathrm{SW}} \\ &= \tfrac{4D^3T_{\mathrm{SW}}^2}{3TL_{\mathrm{B}}^2} U_{\mathrm{B}}U_{\mathrm{in}}^2 \cdot \textstyle\sum_k \frac{[\sin(\omega k T_{\mathrm{SW}})]^2}{U_{\mathrm{B}} - \sqrt{2}U_{\mathrm{IN}}|\sin(\omega k T_{\mathrm{SW}})|} T_{\mathrm{SW}} \\ &\approx \tfrac{2D^3T_{\mathrm{SW}}^2}{3L_{\mathrm{B}}^2} U_{\mathrm{in}}^2 \tfrac{1}{\pi} \textstyle\int_0^{\pi} \frac{\sin^2(\omega t)}{1 - m\sin(\omega t)} d(\omega t) \\ &= \tfrac{2D^3T_{\mathrm{SW}}^2}{3L_{\mathrm{B}}^2} U_{\mathrm{in}}^2 A \end{aligned} \tag{15}$$

From (5), the expression for the square RMS value of i_{LB} can be derived as follows by neglecting the switching frequency:

$$\begin{aligned} \langle \bar{i}_{\mathrm{LB}} \rangle^2_{\mathrm{RMS},T} &= \tfrac{1}{\pi} \textstyle\int_0^{\pi} \left[\frac{D^2T_{\mathrm{SW}}U_{\mathrm{inm}}}{2L_{\mathrm{B}}} \frac{\sin(\omega t)}{1 - m\sin(\omega t)}\right]^2 d(\omega t) \\ &= \tfrac{D^4T_{\mathrm{SW}}^2U_{\mathrm{in}}^2}{2L_{\mathrm{B}}^2} \tfrac{1}{\pi} \textstyle\int_0^{\pi} \left[\frac{\sin(\omega t)}{1 - m\sin(\omega t)}\right]^2 d(\omega t) \\ &= \tfrac{D^4T_{\mathrm{SW}}^2}{2L_{\mathrm{B}}^2} U_{\mathrm{in}}^2 B \end{aligned} \tag{16}$$

where

$$B = \frac{1}{\pi}\int_0^{\pi}\left[\frac{\sin(\omega t)}{1-m\sin(\omega t)}\right]^2 d(\omega t) \tag{17}$$

From Figure 3, the square RMS value of the current at switching frequency on the AC side of the rectifier is equal to the square RMS value of the switching frequency component of i_{LB}, which can be expressed as (18).

$$I_{TPSW}{}^2 = \left\langle \tilde{i}_{LB} \right\rangle_{RMS,T}^2 \tag{18}$$

Next, the square RMS value of i_{LB} at the switching frequency can be obtained by the difference of the square RMS value of the total current i_{LB} and the square RMS value of the current obtained by neglecting the switching frequency [37,39], which can be expressed as

$$\left\langle \tilde{i}_{LB} \right\rangle_{RMS,T}^2 = \langle i_{LB}\rangle_{RMS,T}^2 - \left\langle \bar{i}_{LB} \right\rangle_{RMS,T}^2 \tag{19}$$

The square RMS value of the total current i_{LB} has been obtained as (15), and the square RMS value of the current obtained by neglecting the switching frequency has been obtained as (16); thus, Equation (19) can be derived as

$$\left\langle \tilde{i}_{LB} \right\rangle_{RMS,T}^2 = \langle i_{LB}\rangle_{RMS,T}^2 - \left\langle \bar{i}_{LB} \right\rangle_{RMS,T}^2 = \frac{2D^3T_{SW}^2}{3L_B^2}U_{in}^2 A - \frac{D^4T_{SW}^2}{2L_B^2}U_{in}^2 B \tag{20}$$

From (9), D can be replaced by known parameters U_{in}, P, L_B, and T_{SW}. Thus, according to (9), (18), (20), $I_{TPSW}{}^2$ can be obtained as

$$\begin{aligned} I_{TPSW}{}^2 = \left\langle \tilde{i}_{LB} \right\rangle_{RMS,T}^2 &= \langle i_{LB}\rangle_{RMS,T}^2 - \left\langle \bar{i}_{LB} \right\rangle_{RMS,T}^2 \\ &= \frac{2PT_{SW}}{3L_BU_{in}}\sqrt{\frac{PL_B}{AT_{SW}}} - \frac{P^2B}{2U_{in}{}^2A^2} \end{aligned} \tag{21}$$

So I_{TPSW} can be obtained from (21).

3. Parameter Design

A 130-W prototype is taken as an example for parameter design. The specific design process and a design example are provided in the following.

3.1. Step-by-Step Design Analysis

The filter parameters L_F and C_F are different when the input voltage u_{in} and the input line frequency current i_{inF} show different phase relationships. In addition, the phase relationships are related to the fundamental power factor λ_F. It is necessary to preset λ_F because the process of parameter design is different for different λ_F.

The filter design process can be divided into the following three scenarios:

(a) the input line frequency current is in phase with the input voltage (resistive input current).
(b) the input line frequency current leads the input voltage (capacitive input current).
(c) the input line frequency current lags the input voltage (inductive input current).

The line frequency phasor model circuit of the filter is shown in Figure 6. Its KVL phasor equation is shown in (22).

$$\dot{U}_{in} - \dot{U}_{LFF} - \dot{U}_{TPF} = 0 \tag{22}$$

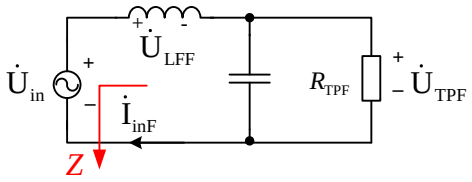

Figure 6. The line frequency phasor circuit.

It can also be expressed as

$$\dot{U}_{in} - \dot{U}_{LFF} = \dot{U}_{TPF} \tag{23}$$

The phasor diagram of the equation for the above three cases is shown in Figure 7a–c. The corresponding λ_F in different cases is shown as follows.

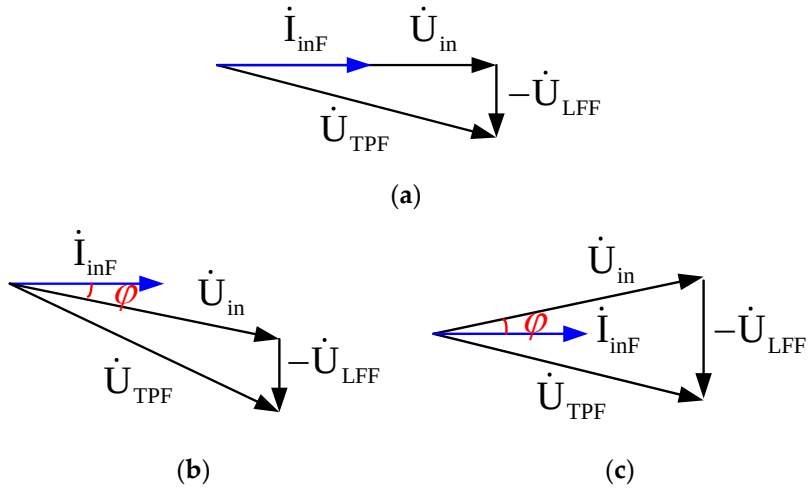

Figure 7. The KVL relationship among voltage phasors. (**a**) Resistive input current. (**b**) Capacitive input current. (**c**) Inductive input current.

(a) Resistive input current

Resistive input current means that the input line frequency current i_{inF} is in phase with the input voltage as shown in Figure 7a, so $\lambda_F = 1$. In addition, the RMS value U_{TPF} is greater than the RMS value U_{in} from Figure 7a, and thus their ratio α can be restricted to $1 < \alpha \leq 1.02$ in this case.

(b) Capacitive input current

In the condition of capacitive input current, the input line frequency current i_{inF} is ahead of the input voltage with an angle of φ as shown in Figure 7b. Obviously, φ is the fundamental power factor angle and $\cos\varphi = \lambda_F < 1$. In this condition, the imaginary part of the input impedance in Figure 6 should be less than zero. The phase between the input voltage u_{in} and the input line frequency current i_{inF} should be as small as possible. Therefore, it can be preset as $0.99 \leq \lambda_F < 1$ according to the analysis in Section 2. Additionally, the RMS value U_{TPF} is greater than the RMS value U_{in} from Figure 7b; thus, preset $1 < \alpha \leq 1.02$ in this case.

(c) Inductive input current

In the condition of inductive input current, the input line frequency current i_{inF} lags the input voltage with the angle φ as shown in Figure 7c. Additionally, φ is the fundamental power factor angle and $\cos\varphi = \lambda_F < 1$. In this condition, the imaginary part of the input impedance in Figure 6 should be greater than zero.

It is worth noting that the largest inductor value is needed in the case of inductive input current among all three scenarios, which results in larger filter volume and lower

power density. Thus, the scenario of inductive input current should be avoided in the filter design. Hence, only the other two scenarios (resistive input current and capacitive input current) are taken into consideration here.

The specific analysis is as follows.

According to the definition of the preset parameters and the circuit parameters in Figures 5–7, the parameters λ_F, α, β and γ can be obtained as follows. Specific derivation is shown in Appendix C.

$$\lambda_F = \frac{R_{TPF}}{\sqrt{R_{TPF}^2 + \omega_L{}^2(L_F + \omega_L{}^2 C_F^2 R_{TPF}^2 L_F - C_F R_{TPF}^2)^2}} \tag{24}$$

$$\alpha = \frac{U_{TPF}}{U_{in}} = \frac{R_{TPF}}{\sqrt{(R_{TPF} - \omega_L{}^2 L_F C_F R_{TPF})^2 + \omega_L{}^2 L_F^2}} \tag{25}$$

$$\beta = \frac{U_{TPSW}}{U_{TPF}} = \frac{I_{TPSW}}{U_{in}} \frac{\omega_{SW} L_F}{|1 - \omega_{SW}{}^2 C_F L_F|} \tag{26}$$

$$\gamma = \frac{I_{inSW}}{I_{inF}} = \frac{I_{TPSW}}{I_{inF}|1 - \omega_{SW}{}^2 C_F L_F|} \tag{27}$$

Next, the values of L_F and C_F should satisfy four Equations (24)–(27), and the way is to solve two of them first.

In the following process, the situation should be excluded when the imaginary part of the input impedance is greater than zero according to the above analysis.

Firstly, L_F and C_F can be solved by combining Equations (24) and (25). It can be obtained as

$$L_F = \frac{-\frac{R_{TPF}}{\omega_L}\sqrt{\frac{1}{\lambda_F^2} - 1} + C_F R_{TPF}^2}{1 + (\omega_L C_F R_{TPF})^2} > 0 \tag{28}$$

$$C_F = \frac{\sqrt{\left(\frac{\alpha}{\lambda_F}\right)^2 - 1}}{\omega_L R_{TPF}} > 0 \tag{29}$$

To express L_F only with known and preset parameters, C_F should be removed from (28). Then substitute (29) into (28), (28) can be derived as

$$L_F = \frac{\frac{R_{TPF}}{\omega_L}\left(-\sqrt{\frac{1}{\lambda_F^2} - 1} + \sqrt{\left(\frac{\alpha}{\lambda_F}\right)^2 - 1}\right)}{\left(\frac{\alpha}{\lambda_F}\right)^2} > 0 \tag{30}$$

Similarly, L_F and C_F can also be solved by combining Equations (26) and (27). Their expression can be obtained as

$$L_F = \frac{\beta U_{in}}{\gamma \omega_{SW} I_{inF}} = \frac{\beta U_{in}{}^2}{\gamma \omega_{SW} P_{in}} > 0 \tag{31}$$

$$C_F = \frac{\gamma P_{in} \pm U_{in} I_{TPSW}}{\beta \omega_{SW} U_{in}{}^2} > 0 \tag{32}$$

In (28), the sign in front of $U_{in} I_{TPSW}$ is determined by the actual conditions, so that C_F is a positive value.

L_F and C_F have been expressed in four expressions (29)–(32), and now their value needs to satisfy these equations at the same time.

The solution is to eliminate L_F through (30) and (31) to get the relationship among λ_F, α, β and γ. Then eliminate C_F through (29) and (32) to get the relationship among λ_F, α, β and γ. Next, solve the above two relationships related to λ_F, α, β and γ. In addition,

select the appropriate value of λ_F, α, β and γ that satisfies the preset conditions. Finally, substitute the value of λ_F, α, β and γ into (29)–(32) to get the value of L_F and C_F. The specific steps are as follows.

From (30) and (31), the relationship between the parameters λ_F, α, β and γ can be obtained as

$$\frac{\frac{R_{TPF}}{\omega_L}\left(-\sqrt{\frac{1}{\lambda_F^2}-1}+\sqrt{\left(\frac{\alpha}{\lambda_F}\right)^2-1}\right)}{\left(\frac{\alpha}{\lambda_F}\right)^2}=\frac{\beta {U_{in}}^2}{\gamma\omega_{SW}P_{in}} \tag{33}$$

Similarly, from (29) and (32), the relationship between the parameters λ_F, α, β and γ can be obtained as

$$\frac{\sqrt{\left(\frac{\alpha}{\lambda_F}\right)^2-1}}{\omega_L R_{TPF}}=\frac{\gamma P_{in}\pm U_{in}I_{TPSW}}{\beta\omega_{SW}{U_{in}}^2} \tag{34}$$

It is worth noting that (24) and (25) are derived from the circuit in Figure 5b, and the LC filter parameters only relate to λ_F and α. Similarly, (26) and (27) are derived from the circuit in Figure 5c, and the LC filter parameters only relate to β and γ. To satisfy the performance requirements, the constraints of the above four preset parameters should be satisfied at the same time according to the operation principle of SSC. Therefore, the parameters L_F and C_F should be jointly determined by (24)–(27). Through the above derivation, once the parameters λ_F, α, β and γ are chosen, L_F and C_F can be determined.

3.2. A Design Example

The specifications of the single-stage high-frequency AC/AC converter are as follows. Table 2 lists the system parameters for the design example of the LC input filter.

Table 2. Prototype specifications.

Specifications	**Value**
Input voltage u_{in}	220 V_{AC}/50 Hz
Output Power $P = P_{in}$	130 W
Switching frequency f_{SW}	100 kHz
$m = U_{inm}/U_B$	0.8
Boost inductor L_B	150 μH
Turns ratio N_R	1.1
Energy storage capacitor C_B	110 μF
Series resonant inductor L_S	75 μH
Parallel resonant inductor L_P	12 μH
Series resonant capacitor C_S	42 nF
Parallel resonant capacitor C_P	145 nF
Output voltage u_{AC}	45 V
Output load R_L	15.6 Ω

According to the derivation of (24)–(34), the entire design procedure for LC input filter is shown in the flowchart in Figure 8. The discussion is as follows.

Firstly, the precise design method is based on the restrictions of the input harmonic currents, so parameters λ_F, α, β and γ are preset in a variation range. R_{TPF} and I_{TPSW} appear in the expression of λ_F, α, β and γ in (24)–(27), so they should be calculated first. The values of L_F and C_F should satisfy four Equations (24)–(27) at the same time, and the solution is to eliminate L_F and C_F to get two relationships among λ_F, α, β and γ. Taking $\lambda_F = 0.9$ after analysis, two 3D Figures about (α, β, γ) can be obtained. Select one point in the intersection curve of two 3D Figures, the corresponding value of (α, β, γ) can be obtained. Then, L_F and C_F can be determined.

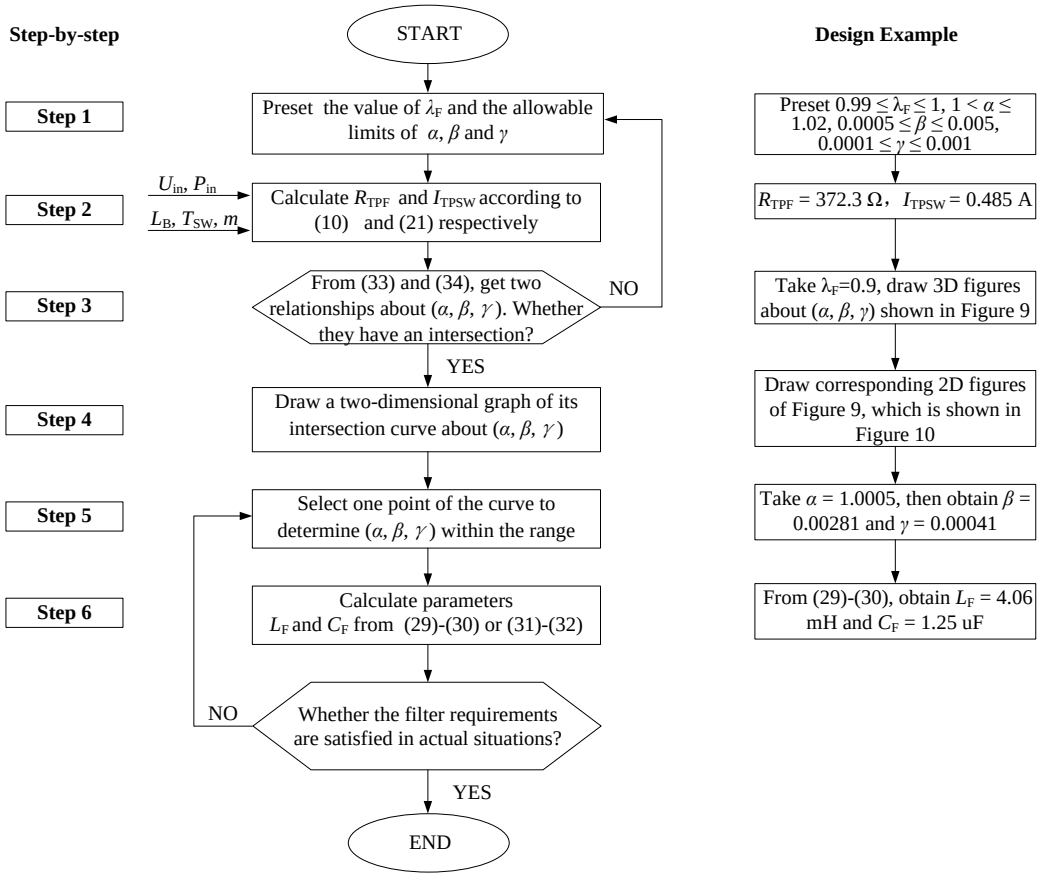

Figure 8. Design flow chart for LC low–pass filter.

The specific step-by-step design process is in the following.

Step 1: Firstly, according to the analysis in Section 2, the variation range of parameters λ_F, α, β and γ are preset as $0.99 \le \lambda_F \le 1$, $1 < \alpha \le 1.02$, $0.0005 \le \beta \le 0.005$, $0.0001 \le \gamma \le 0.001$. To simplify the calculation, $\lambda_F = 0.99$ is taken as an example in the design process, which corresponds to the capacitive input current condition. Next, it is only needed to determine the combination of (α, β, γ) according to (33)–(34). In addition, the influence of λ_F is analyzed at the end of this section.

Step 2: Except for parameters known and preset above, R_{TPF} and I_{TPSW} should be calculated below from (10) and (21).

$$R_{TPF} = 372.3\ \Omega,\ I_{TPSW} = 0.485\ \text{A} \tag{35}$$

Step 3: Equations (33) and (34) can be sorted out as (36) and (37). Substitute the above parameters into (36) and (37), and two relationships about (α, β, γ) can be obtained. Draw two 3D Figures about (α, β, γ), which is shown in Figure 9. Check if the two 3D figures have an intersection.

$$\beta = \frac{\gamma \omega_{SW} P_{in} \frac{R_{TPF}}{\omega_L} \left(-\sqrt{\frac{1}{\lambda_F^2} - 1} + \sqrt{\left(\frac{\alpha}{\lambda_F}\right)^2 - 1} \right)}{{U_{in}}^2 \left(\frac{\alpha}{\lambda_F}\right)^2} \tag{36}$$

$$\beta = \frac{\omega_L R_{TPF} (\gamma P_{in} \pm U_{in} I_{TPSW})}{\omega_{SW} {U_{in}}^2 \sqrt{\left(\frac{\alpha}{\lambda_F}\right)^2 - 1}} \tag{37}$$

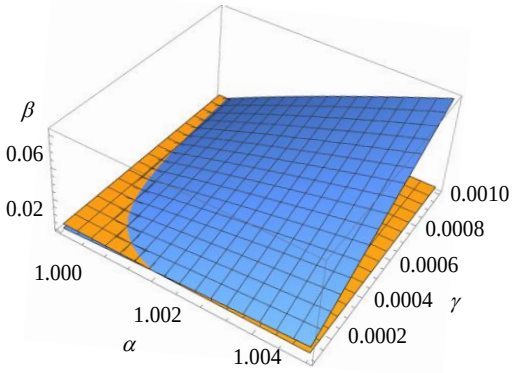

Figure 9. The 3D figures about (α, β, γ).

Step 4: If the two 3D figures have intersection, draw 2D figures of the intersection curve. Otherwise, reset the range of above parameters to get the intersection curve. For given parameters, the intersection curve can be obtained in Figure 10.

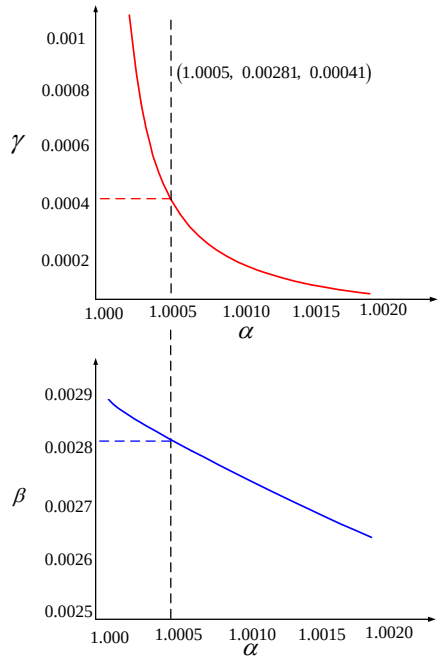

Figure 10. The corresponding 2D figures about (α, β, γ).

Step 5: Selecting one point on the intersection curve, the corresponding value of (α, β, γ) can be obtained.

Step 6: L_F and C_F can be determined by (29)–(30) or (31)–(32).

According to the above analysis, taking α = 1.0005 as an example in Figure 10, it can be derived that β = 0.00281 and γ = 0.00041. Correspondingly, L_F and C_F can be determined by (29)–(30), that is, L_F = 4.06 mH and C_F = 1.25 uF.

In addition, the range of L_F and C_F can be also determined. According to (29) and (30), L_F and C_F are only related to α with a fixed λ_F. The relationship between L_F and and α is shown in Figure 11, and the relationship between C_F and α is shown in Figure 12. It can be seen that L_F varies greatly with α while C_F varies small.

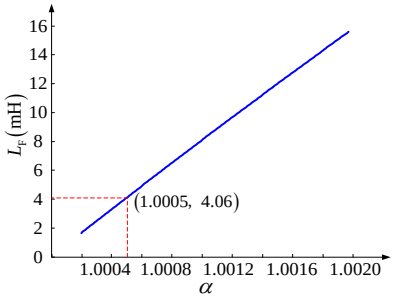

Figure 11. The relationship between L_F and α.

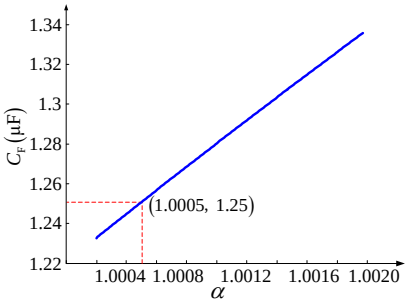

Figure 12. The relationship between C_F and α.

Next, the influence of λ_F is considered. The corresponding L_F and C_F are listed in Table 3 when λ_F changes at the same operation point (α = 1.005). It can be seen that L_F increases and C_F decreases with increasing λ_F. The size of the filter is mainly determined by L_F. The filter volume is larger and power density is lower when λ_F increases. L_F is equal to 38.21 mH when λ_F = 1, resulting in a large inductor. Moreover, β exceeds the preset range when λ_F is greater than 0.998 as shown in Table 3. Then α needs to be increased to cause β to be within the preset range in this case. However, increasing α will result in larger L_F. Therefore, the fundamental power factor λ_F is sacrificed a little bit for smaller filter size, which is taken as 0.99.

Table 3. The corresponding L_F and C_F when input fundamental power factor changes.

λ_F	(α, β, γ)	L_F (mH)	C_F (uF)
0.990	(1.005, 0.00281, 0.00041)	4.06	1.25
0.991	(1.005, 0.00296, 0.00041)	4.28	1.19
0.992	(1.005, 0.00313, 0.00040)	4.64	1.12
0.993	(1.005, 0.00333, 0.00040)	4.93	1.05
0.994	(1.005, 0.00358, 0.00040)	5.30	0.98
0.995	(1.005, 0.00390, 0.00040)	5.78	0.90
0.996	(1.005, 0.00431, 0.00040)	6.38	0.81
0.997	(1.005, 0.00489, 0.00040)	7.24	0.72
0.998	(1.005, 0.00579, 0.00039)	8.79	0.61
0.999	(1.005, 0.00749, 0.00037)	11.99	0.47
1.000	(1.005, 0.01297, 0.00021)	38.21	0.38

4. Sensitivity Analysis of LC Filter

The analysis of the design of L_F and C_F was performed in the previous section. The requirements of SSC can be satisfied with the L_F and C_F designed above. However, parameters may need to be adjusted in practical applications in terms of volume, loss, power density, etc. There is a correlation between L_F and C_F, and their value will also have an impact on the performance. In order to achieve this, the values of (α, β, γ) are changed to correspond to L_F and C_F. Therefore, it is necessary to qualitatively evaluate the influence of α, β and γ on the corresponding L_F and C_F. The sensitivity of the input filter to parameters α, β and γ is analyzed below.

The formula of the normalized sensitivity S_x^T is as follows. When x has a small change Δx, S_x^T is the ratio of the relative change of function T to the relative change of x, where Δx infinitely approach zero.

$$S_x^T = \frac{x}{T}\frac{\partial T}{\partial x} \tag{38}$$

From (30) and (31), L_F can be expressed as

$$L_F = \frac{\frac{R_{TPF}}{\omega_L}\left(-\sqrt{\frac{1}{\lambda_F^2}-1}+\sqrt{\left(\frac{\alpha}{\lambda_F}\right)^2-1}\right)}{\left(\frac{\alpha}{\lambda_F}\right)^2} = \frac{\beta {U_{in}}^2}{\gamma \omega_{SW} P_{in}} \tag{39}$$

From (29) and (32), C_F can be expressed as

$$C_F = \frac{\sqrt{\left(\frac{\alpha}{\lambda_F}\right)^2-1}}{\omega_L R_{TPF}} = \frac{\gamma P_{in} \pm U_{in} I_{TPSW}}{\beta \omega_{SW} {U_{in}}^2} \tag{40}$$

According to the design process in Section 3, the working point (α, β, γ) = (1.0005, 0.00281, 0.00041) and λ_F = 0.99 is chosen. Next, the normalized sensitivity of L_F to α, β and γ is analyzed at this point.

From (39), this can be derived as

$$\begin{cases} S_\alpha^{L_F} = \frac{\alpha}{L_F}\frac{\partial L_F}{\partial \alpha} = \frac{\alpha}{\frac{372.3}{100\pi}\left(-\sqrt{\frac{1}{0.99^2}-1}+\sqrt{\frac{1.0005^2}{0.99^2}-1}\right)}{\frac{1.0005^2}{0.99^2}}\frac{\partial L_F}{\partial \alpha} = 1975.26 \\ S_\beta^{L_F} = \frac{\beta}{L_F}\frac{\partial L_F}{\partial \beta} = \frac{\beta}{\frac{\beta}{\gamma}\frac{220^2}{2\pi\times 10^5\times 130}}\frac{220^2}{\gamma 2\pi\times 10^5\times 130} = 1 \\ S_\gamma^{L_F} = \frac{\gamma}{L_F}\frac{\partial L_F}{\partial \gamma} = \frac{\gamma}{\frac{\beta}{\gamma}\frac{220^2}{2\pi\times 10^5\times 130}}\frac{-\beta 220^2}{\gamma^2 2\pi\times 10^5\times 130} = -1 \end{cases} \tag{41}$$

Similarly, the normalized sensitivity of C_F to α, β and γ can be calculated from (40).

$$\begin{cases} S_\alpha^{C_F} = \frac{\alpha}{C_F}\frac{\partial C_F}{\partial \alpha} = \frac{\alpha}{\frac{\alpha^2}{0.99^2}-1}\frac{\partial C_F}{\partial \alpha} = -\frac{\alpha}{0.99^2} = -1.021 \\ S_\beta^{C_F} = \frac{\beta}{C_F}\frac{\partial C_F}{\partial \beta} = \frac{\beta}{\frac{\gamma\times 130+220\times 0.485}{\beta 2\pi\times 10^5\times 220^2}}\frac{\partial C_F}{\partial \beta} = -1 \\ S_\gamma^{C_F} = \frac{\gamma}{C_F}\frac{\partial C_F}{\partial \gamma} = \frac{\gamma}{\frac{\gamma\times 130+220\times 0.485}{\beta 2\pi\times 10^5\times 220^2}}\frac{\partial C_F}{\partial \gamma} = 0.0005 \end{cases} \tag{42}$$

According to the sensitivity analysis, the normalized sensitivities of L_F and C_F to α, β and γ are quantitatively analyzed above. The following results can be obtained.

① As shown in (41), $S_\alpha^{L_F} > 0$, $S_\beta^{L_F} > 0$, $S_\gamma^{L_F} < 0$. It can be seen that L_F increases with increasing α and β. In addition, L_F decreases with increasing γ.

② Similarly, $S_\alpha^{C_F} < 0$, $S_\beta^{C_F} < 0$, $S_\gamma^{C_F} > 0$. It can be seen that C_F decreases with the increase of α and β. In addition, C_F increases with the increase of γ.

③ It can also be seen that α has the greatest impact on L_F, and the normalized sensitivity of β and γ to L_F are similarly small. In addition, α and β have similar influences on C_F, and γ has the smallest effect on C_F. As α has such a big influence on L_F, Figure 13 shows the relationship between $S_\alpha^{L_F}$ and α.

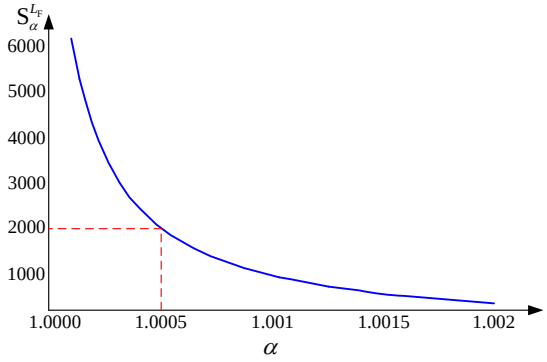

Figure 13. The relationship between $S_\alpha^{L_F}$ and α.

It can be seen that $S_\alpha^{L_F}$ is very large in the range of α, indicating that α has a greater influence on L_F. In addition, it can be seen that the range of C_F is small, while the range of L_F is large, from Figures 11 and 12, which is consistent with the above results.

According to the above analysis results, L_F and C_F can be changed according to the corresponding change trend in practical applications. More attention should be paid to L_F, and it is more reasonable to adjust α at first when adjusting the value of L_F. For example, if the inductor L_F needs to be changed in terms of volume, α can be adjusted preferentially, and C_F can be obtained accordingly, completing the adjustment process. The impact on performance can be reduced to a minimum in this way. In conclusion, sensitivity analysis provides a method that can adjust parameters to the expected value accurately, and the performance can be satisfied at the same time. It is of great value in practical applications and provide a guide in engineering applications.

5. Simulation Results

A 130 W prototype is built to verify parameter design. The input LC filter and the corresponding single-stage high frequency AC/AC converter is shown in Figure 14. The specifications of the simulation and experimental prototype are consistent with Table 2.

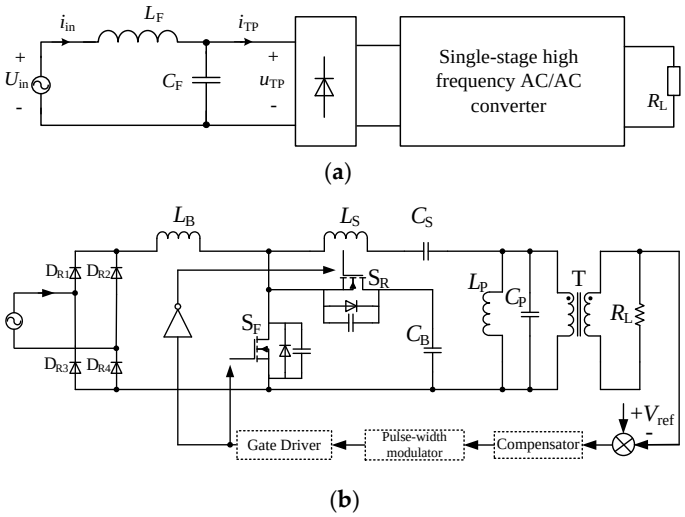

Figure 14. The input LC filter and the single−stage AC/AC converter with its control block diagram. (**a**) The input LC filter. (**b**) The single−stage AC/AC converter with its control block diagram.

As for the closed-loop control, the output voltage is sampled and compared with the reference signal to get the error signal. After the error signal is processed by the PI compensator, a modulated signal is obtained, which is compared with the triangular carrier, then PWM signal can be obtained. Therefore, the closed-loop control on the output voltage can be achieved. The corresponding control block diagram is shown in Figure 14b.

From the parameter design process, it can be seen R_{TPF} and I_{TPSW} need to be calculated first. The results of R_{TPF} and I_{TPSW} have been shown in (34) with R_{TPF} = 372.3 Ω, I_{TPSW} = 0.485 A. In addition, the related preset and filter parameters are concluded in Table 4. The interaction between the LC filter and the AC/AC converter involves above parameters. In addition, these preset parameters can be accurately verified via simulations.

Table 4. Preset and filter parameters.

Symbol	Value
λ_F	0.99
(α, β, γ)	(1.0005, 0.00281, 0.00041)
L_F	4.06 mH
C_F	1.25 uF

The simulation waveforms are obtained by PSIM, which is a simulation software package. The simulation input and output parameters are consistent with Table 2. Through PSIM simulation, the voltage and current before and after filtering are shown in Figure 15. Figure 15a,b show the waveforms of line voltage u_{in} and input current i_{in}, respectively, and the input current is ahead of the line voltage, so $\lambda_F < 1$. Figure 15c,d give the input voltage u_{TP} and the input current i_{TP} of the rectifier bridge, respectively. It can be seen that the higher harmonics in the current i_{TP} can be mostly filtered out.

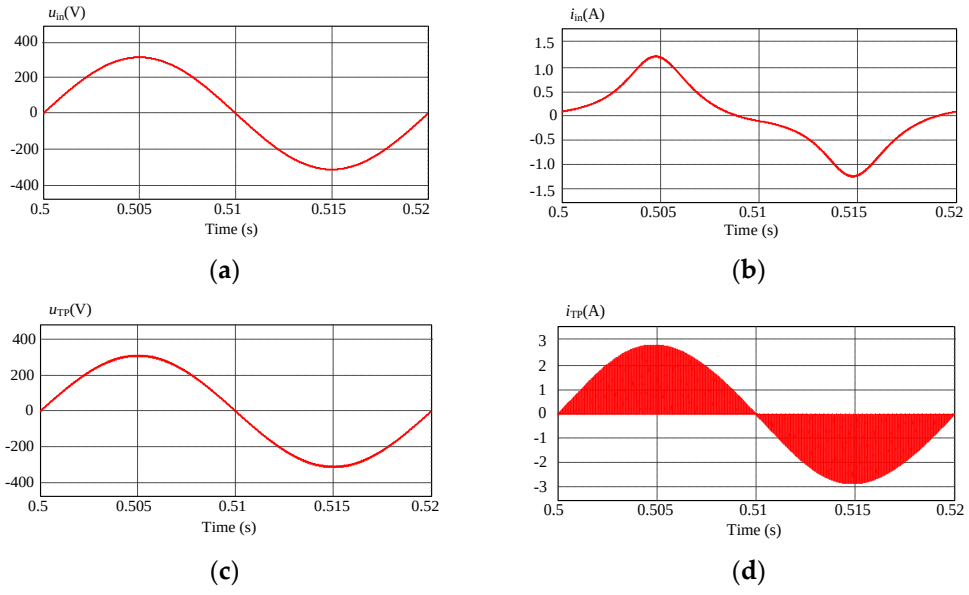

Figure 15. The simulation waveforms. (**a**) Input voltage uin. (**b**) Input current i_{in}. (**c**) PFC input voltage u_{TP}. (**d**) PFC input current i_{TP}.

Next, it is necessary to analyze the harmonic content more accurately to verify the parameter design. The data of waveform i_{in}, u_{TP}, and i_{TP} can be obtained by PSIM. Then these data can be processed by FFT analysis with MATLAB, and the frequency spectrum of the above simulation waveforms can be obtained as shown in Figure 16. The frequency spectrum of the input current i_{in}, the input voltage u_{TP} and input current i_{TP} of rectifier bridge are shown in Figure 16a–c, respectively. It can be seen from Figure 16a that the harmonics in the input current are mainly the third, fifth, seventh and other low-order harmonics, and the filter parameters have little effect on it.

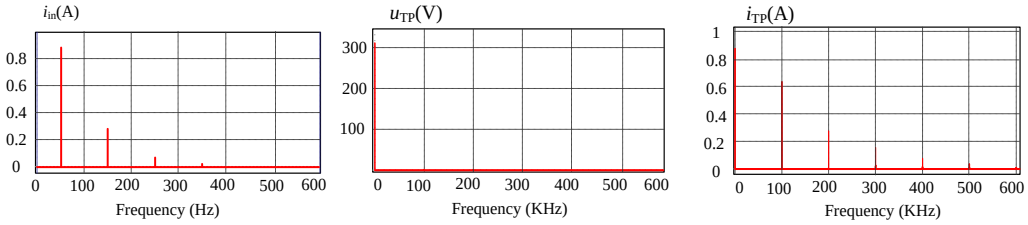

(**a**) (**b**) (**c**)

Figure 16. The frequency spectrum of the simulation waveforms. (**a**) The input current i_{in}. (**b**) The input voltage u_{TP}. (**c**) The input current i_{TP}.

In addition, the peak values of the input current at fundamental frequency respectively obtained from Figure 16a,c are 0.878 A and 0.869 A, and that of the input current calculated from (6) is 0.836 A. The above three values are almost equal to each other.

In Figure 16c, the peak value of current at switching frequency is 0.617 A, and that of the current at 200 kHz, 300 kHz and 400 kHz are 0.267 A, 0.148 A, and 0.082 A, respectively, so the RMS value of above four can be calculated and the value is 0.491 A, which is equal to I_{TPSW} = 0.485 A with an acceptable error.

Similarly, the preset parameters are verified as follows.

Parameter α: It can be seen from Figure 16b that the peak value of u_{TP} at fundamental frequency U_{TPFm} is about 311.291 V. Therefore, the ratio of the corresponding effective value U_{TPF} to the effective value of the input voltage U_{in} is α = 1.00053, which conforms to the preset range of $1 < \alpha \leq 1.002$.

Parameter β: In Figure 16b, the peak value of u_{TP} at the switching frequency U_{TPSWm} is about 0.871 V, and the ratio of the corresponding effective value U_{TPSW} to the effective value of the input voltage U_{in} can be obtained as β = 0.002798, which conforms to the preset range of $0.0005 \leq \beta \leq 0.005$.

Parameter γ: In Figure 16a, the peak value of i_{in} at the switching frequency component I_{inSWm} is about 0.000335 A, and the ratio of the corresponding effective value I_{inSW} to its effective value at fundamental frequency I_{inF} is γ = 0.000401, which conforms to the preset range of $0.0001 \leq \gamma \leq 0.001$.

In addition, the input power factor is 0.949 on the basis of the simulation calculations. The total harmonic distortion (THD) of the input current is 25.8%, and the harmonic of each order meets the requirements of IEC61000-3-2 Class C, as shown in Figure 17. It can be seen that the above simulation results verify the correctness of the analysis and the validity of the design method.

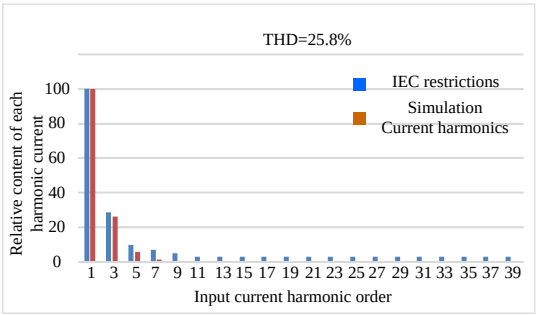

Figure 17. The content of each order harmonic component in the input current through simulation.

6. Experimental Results

A 130 W experimental prototype is established to verify parameter design. The specifications of the experimental prototype are consistent with Tables 2 and 4. Figure 18 shows a photograph of the experimental prototype. The control circuit is shown in Figure 14b, and the control board is TMS320F28335. The model of diodes D_{R1}-D_{R4} was MUR860, and

the model of switches S_F and S_R was IPP60R099C7. The output load is pure resistive, and the output voltage is constant because of the closed-loop control.

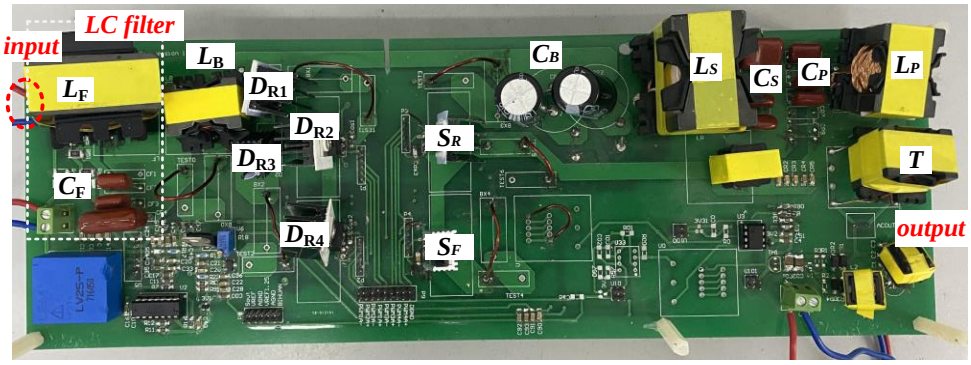

Figure 18. The prototype of the single-stage AC/AC converter.

For capacitor C_F, three capacitors are connected in parallel to provide the designed value of 1.25 uF. Considering the limited selection during the experiment, there is a certain deviation between the experimental value and the design value. In addition, the values of three parallel capacitors in the experiment are 0.82, 0.22 and 0.22 uF, respectively.

For inductor L_F, the implementation design process of L_F is shown in Appendix B.

Figure 19a–c below show the measured input current i_{in} after filtered and current i_{TP} at different input voltages. It can be seen that the envelope of i_{TP} is sinusoidal and in phase with u_{in}, which is consistent with analysis in Section 2. Additionally, it can be seen that the higher harmonics in the current i_{TP} are greatly suppressed.

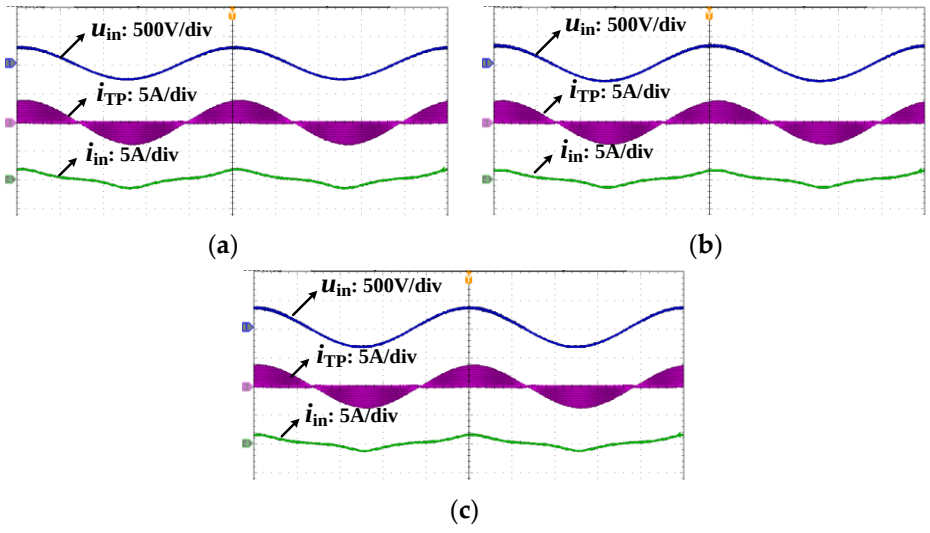

Figure 19. The measured waveforms of input current i_{in} after filtered and current i_{TP} at different input voltages. (**a**) u_{in} = 198 V. (**b**) u_{in} = 220 V. (**c**) u_{in} = 242 V.

Figure 20 shows the enlarged input voltage u_{in} and filtered current i_{in}. The rated input voltage u_{in} is 220 V. To present a more comprehensive result, waveforms under different input voltages are presented. From Figure 20a–c, the current zero-crossing point is ahead of the input voltage zero-crossing point. Therefore, it can be seen that the input current is always ahead of the input voltage as the input voltage changes. The capacitive input current case is satisfied, and corresponding λ_F is always less than 1, which is consistent with analysis in Section 3.

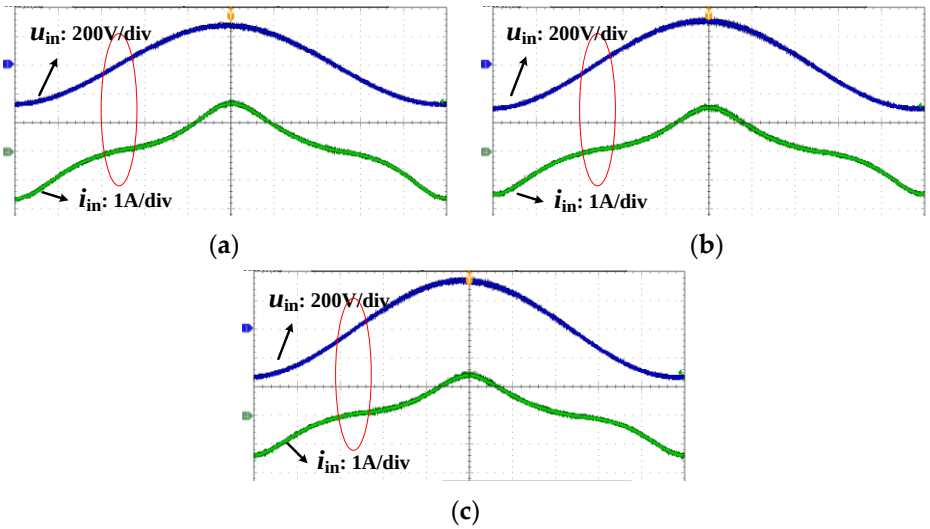

Figure 20. The enlarged waveforms of input voltage and current of Figure 19 at different input voltages. (**a**) u_{in} = 198 V. (**b**) u_{in} = 220 V. (**c**) u_{in} = 242 V.

In addition, the experimental input power factor is about 0.935 at rated state when LC filter is involved to filter out the high-order harmonic components in the current i_{TP}. The result meets the requirement of Energy Star [40].

Figure 21 shows the frequency spectrum of the input current obtained through experiment. It shows the content of each harmonic contained in the input current i_{in}. Additionally, a comparison between the harmonic content obtained by the experiment and simulation is also presented in Figure 21. The simulation and experimental input currents mostly contain three, five, and seven harmonics. The experimental harmonic distribution is roughly consistent with the simulation results. The contents of the corresponding harmonics are roughly the same. Finally, the experimental input current THD is about 26.4%, which is slightly larger than the simulation results. In addition, IEC61000-3-2 Class C restrictions are marked in blue in Figure 21, and it can be seen that experimental current harmonics meet the IEC restrictions, which is also close to the simulation results. All in all, the experimental results verify the validity of the design method.

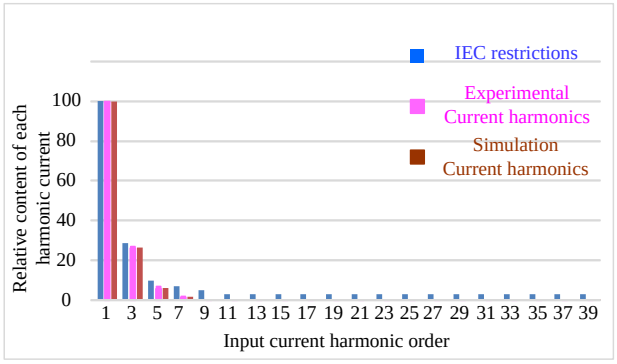

Figure 21. The experimental frequency spectrum of the input current compared with IEC and simulation.

In order to completely present the experimental results, Figure 22 shows the experimental waveforms of the prototype at rated power. Figure 22a shows the switching voltage u_{SF} and the switching current i_{SF} at P = 130 W and u_{in} = 220 V. The switching voltage of S_R and the corresponding current are shown in Figure 22b. It can be seen that i_{SF} and i_{SR} are less than zero before the corresponding switch is turned on, and it means that their anti-parallel diodes are forced to conduct, so S_F and S_R can achieve zero-voltage switching

(ZVS). Figure 22c represents the storage capacitor voltage u_B with u_{in} = 220 V. The average value of u_B is less than 400 V. Additionally, Figure 22d shows the measured output voltage u_{AC} with u_{in} = 220 V. It can be seen that the sinusoidal output voltage can be obtained with f_{SW} = 100 kHz.

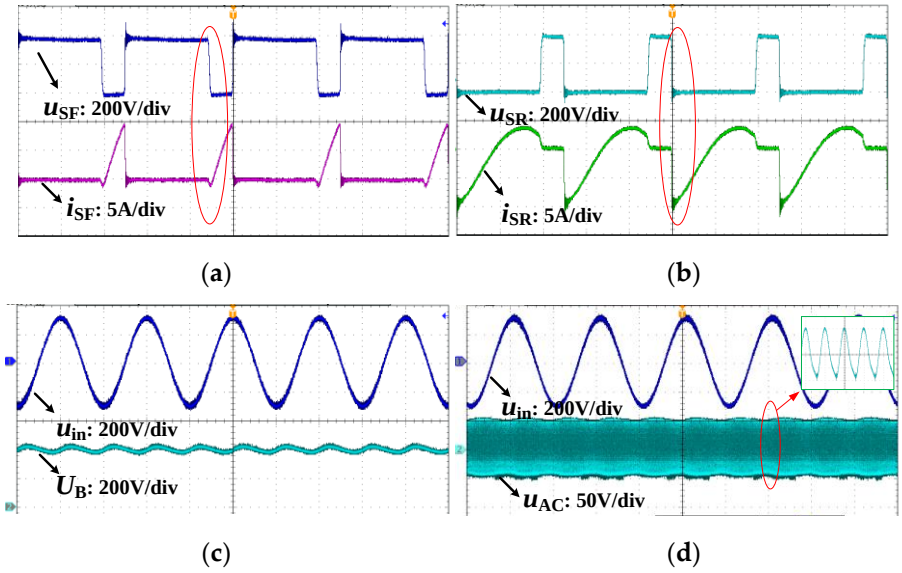

Figure 22. The experimental waveforms. (**a**) The waveforms of u_{SF} and i_{SF}. (**b**) The waveforms of u_{SR} and i_{SR}. (**c**) The voltage U_B at u_{in} = 220 V. (**d**) The output voltage u_{AC}.

7. Conclusions

In this paper, the AC side equivalent circuit of the single-stage converter is obtained using the superposition principle. Then, the RMS value of the input current on the AC side of the rectifier bridge is quantitatively calculated. Next, according to the known and preset parameters, the LC low-pass filter is designed in detail. A quantitative design method for the input filter was proposed. Meanwhile, the sensitivity of the inductor and capacitor in the filter were analyzed. The parameters α, β and γ are preset to a range characterizing the performance of the LC filter. According to the PSIM simulation results, the preset parameters α = 1.00053, β = 0.002798, γ = 0.000401 all conforms to the preset range. The correctness of the proposed design method can be verified. Finally, a 130-W prototype is established. Its measured input power factor is around 0.935 and its input current THD is about 26.4%, and the higher harmonics in the input current can be mostly filtered out, which satisfies IEC61000-3-2 Class C restrictions. The contributions of this paper can be summarized as follows.

(1) The paper offers a quantitative parameter design method with several references. Therefore, me references just give the direction on how to design and adjust or design procedure with try and error method, which is complicated and time-consuming. The proposed method is a programmatic step-by-step design method, which is an easy-to-use tool for designing an LC input filter. Meanwhile, the precise design method is based on the restrictions of the input harmonic currents, so an accurate analytical design procedure is presented.
(2) The sensitivity analysis provides a method that can accurately adjust input filter parameters to the expected value, and the performance can be satisfied at the same time.

It is also shown the inductor should be paid more attention in practical applications. It is more reasonable to adjust α first when adjusting the value of L_F. It is of great value in practical applications and provides a direction in engineering applications.

Author Contributions: Conceptualization, methodology, data curation, writing Q.H., Q.L.; analysis, software, experiment Q.H., L.L., M.Q. All authors have read and agreed to the published version of the manuscript.

Funding: This research was funded by National Natural Science Foundation of China, grand number 51577019.

Institutional Review Board Statement: Not applicable.

Informed Consent Statement: Not applicable.

Data Availability Statement: Not applicable.

Conflicts of Interest: The authors declare no conflict of interest.

Appendix A

To improve readability, the symbols used in the design process are listed and added as an Appendix.

Symbol	Explanation
u_{in}	input voltage
U_{in}	the RMS value of u_{in}
u_{TP}	the voltage drop across the AC side of the diode rectifier bridge
u_{TPF}	the component of u_{TP} at the grid frequency
U_{TPF}	the RMS value of u_{TPF}
U_{TPFm}	the amplitude value of U_{TPF}
u_{TPSW}	the harmonic component of u_{TP} at the switching frequency
U_{TPSW}	the RMS value of u_{TPSW}
i_{in}	input current
i_{inF}	the component of i_{in} at the grid frequency
I_{inF}	the RMS value of i_{inF}
i_{inSW}	the component of i_{in} at the switching frequency
I_{inSW}	the RMS value of i_{inSW}
i_{TP}	the input current of the AC side of the diode rectifier bridge
i_{TPF}	the component of i_{TP} at the grid frequency
I_{TPF}	the RMS value of i_{TPF}
i_{TPSW}	the component of i_{TP} at the switching frequency
I_{TPSW}	the RMS value of i_{TPSW}
R_{TPF}	an equivalent resistor of the output of the LC filter at the grid frequency
U_B	the voltage across the stored-energy capacitor
m	$m = U_{TPFm}/U_B$
φ	the input grid frequency current i_{inF} lags the input voltage with angle φ
λ_F	the fundamental power factor $\lambda_F = \cos\varphi$
α	$\alpha = U_{TPF}/U_{in}$
β	$\beta = U_{TPSW}/U_{TPF}$
γ	$\gamma = I_{inSW}/I_{TPF}$

Appendix B

The implementation design process of the inductor L_F is shown below.

According to the simulation results, the maximum of the input current is I_{max} = 1.2 A, and the RMS value of the input current is I = 0.63 A. The value of L_F is 4.06 mH.

The EE magnetic core is adopted because it has good heat dissipation conditions, and its empirical value of current density is J = 420 A/cm^2. Its current density proportional coefficient is K_j = 0.013 [41]. The maximum magnetic swing ΔB_{max} can be set to 0.28 T. According to AP method (area product method) shown in [41], the formula of the selection of the inductor core is

$$AP = \left[\frac{L\Delta I}{\Delta B_{max}} \cdot \frac{I_{max}}{K_j}\right]^{4/3} = \left[\frac{4.06 \times 10^{-3} \times 1.2}{0.28} \cdot \frac{1.2}{0.013}\right]^{4/3} = 1.844\ \text{cm}^4$$

Select the magnetic core whose AP value is greater than and closest to 1.844 cm^4 by looking it up the table [41]. Therefore, EE40 is selected and its AP = 2.2 cm^4.

Then turns N of the inductor L_F is

$$N = \frac{L\Delta I_{max}}{\Delta B_{max} A_e} = \frac{4.06 \times 10^{-3} \times 1.2}{0.28 \times 127 \times 10^{-6}} = 135$$

where A_e is the EE40 core column cross-sectional area, and A_e = 127 × 10^{-6} mm^2.

Next, the air gap length δ is calculated as

$$\delta = \frac{\mu_0 N^2 A_\delta}{L} \times 10^{-2} = \frac{4\pi \times 10^{-7} \times 135^2 \times 127 \times 10^{-2}}{4.06 \times 10^{-3}} \times 10^{-2} = 0.0727\,\text{cm}$$

Finally, the conductor bare wire cross-section A_L can be calculated according to the current density.

$$A_L = \frac{I}{J} = \frac{0.63}{420}\,\text{cm}^2 = 1.5 \times 10^{-3}\,\text{cm}^2 = 0.15\,\text{mm}^2$$

Looking up the AWG table [41], the available wire type is AWG-25, and its cross-sectional diameter is 0.1623 mm^2.

Appendix C

To improve the readability and make the paper clearer, the analysis and derivation of Equations (24)–(27) in the paper are added. Actually, Equations (24)–(27) are obtained according to the basic circuit principle of Figures 5–7.

For Equation (24), λ_F is the fundamental power factor and λ_F = cosφ as shown in Figure 7. As shown in Figure 6, if the equivalent impedance of the fundamental frequency phasor circuit is $Z = R + jX$, it can be derived that $\lambda_F = R/\sqrt{R^2 + X^2}$.

From Figure 6, the equivalent impedance Z can be derived as

$$Z = j\omega_L L_F + \frac{\frac{1}{j\omega_L C_F} R_{TPF}}{\frac{1}{j\omega_L C_F} + R_{TPF}} = \frac{R_{TPF} + j(\omega_L L_F + {\omega_L}^3 {C_F}^2 L_F {R_{TPF}}^2 - \omega_L C_F {R_{TPF}}^2)}{1 + {\omega_L}^2 {C_F}^2 {R_{TPF}}^2}$$

Therefore, the fundamental power factor λ_F is deduced as

$$\lambda_F = \frac{R}{\sqrt{R^2 + X^2}} = \frac{R_{TPF}}{\sqrt{R_{TPF}^2 + {\omega_L}^2 (L_F + {\omega_L}^2 C_F^2 R_{TPF}^2 L_F - C_F R_{TPF}^2)^2}}$$

For Equation (25), according to Figure 6, the ratio of voltage U_{TPF} to U_{in} is equal to the absolute value of the parallel impedance of the resistor and capacitor divided by that of the input impedance Z. Therefore, it can be deduced as

$$\alpha = \frac{U_{TPF}}{U_{in}} = \left| \frac{\frac{\frac{1}{j\omega_L C_F} R_{TPF}}{\frac{1}{j\omega_L C_F} + R_{TPF}}}{j\omega_L L_F + \frac{\frac{1}{j\omega_L C_F} R_{TPF}}{\frac{1}{j\omega_L C_F} + R_{TPF}}} \right| = \left| \frac{R_{TPF}}{(1 + j\omega_L C_F R_{TPF}) j\omega_L L_F + R_{TPF}} \right| = \frac{R_{TPF}}{\sqrt{(R_{TPF} - {\omega_L}^2 L_F C_F R_{TPF})^2 + {\omega_L}^2 L_F^2}}$$

For Equation (26), the relationship between U_{TPSW} and I_{TPSW} needs to be derived first. According to Figure 5c, the ratio of voltage U_{TPSW} to current I_{TPSW} is equal to the absolute value of parallel impedance of inductor and capacitor Z_1.

So it can be obtained as

$$\frac{U_{TPSW}}{I_{TPSW}} = \left| \frac{j\omega_L L_F \frac{1}{j\omega_L C_F}}{j\omega_L L_F + \frac{1}{j\omega_L C_F}} \right| = \frac{\omega_L L_F}{|1 - {\omega_L}^2 L_F C_F|}$$

Then, Equation (26) can be deduced as

$$\beta = \frac{U_{\mathrm{TPSW}}}{U_{\mathrm{TPF}}} = \frac{I_{\mathrm{TPSW}}}{U_{\mathrm{in}}} \frac{\omega_{\mathrm{L}} L_{\mathrm{F}}}{|1 - {\omega_{\mathrm{L}}}^2 L_{\mathrm{F}} C_{\mathrm{F}}|}$$

For Equation (27), according to Figure 5c, the ratio of current I_{inSW} to current I_{TPSW} is equal to the absolute value of capacitor divided by the absolute value of parallel impedance of inductor and capacitor Z_1, that is:

$$\frac{I_{\mathrm{inSW}}}{I_{\mathrm{TPSW}}} = \left| \frac{\frac{1}{\mathrm{j}\omega_{\mathrm{L}} C_{\mathrm{F}}}}{\mathrm{j}\omega_{\mathrm{L}} L_{\mathrm{F}} + \frac{1}{\mathrm{j}\omega_{\mathrm{L}} C_{\mathrm{F}}}} \right| = \frac{1}{|1 - {\omega_{\mathrm{L}}}^2 L_{\mathrm{F}} C_{\mathrm{F}}|}$$

Then Equation (27) can be deduced as

$$\gamma = \frac{I_{\mathrm{inSW}}}{I_{\mathrm{inF}}} = \frac{I_{\mathrm{TPSW}}}{I_{\mathrm{inF}} |1 - {\omega_{\mathrm{SW}}}^2 C_{\mathrm{F}} L_{\mathrm{F}}|}$$

References

1. Mayordomo, J.G.; Beites, L.F.; Yang, X.; Xu, W. A Detailed Procedure for Harmonic Analysis of Three-Phase Diode Rectifiers Under Discontinuous Conduction Mode and Nonideal Conditions. *IEEE Trans. Power Deliv.* **2018**, *33*, 741–751. [CrossRef]
2. Du, Y.; Wang, J.; Wang, G.; Huang, A.Q. Modeling of the High-Frequency Rectifier With 10-kV SiC JBS Diodes in High-Voltage Series Resonant Type DC–DC Converters. *IEEE Trans. Power Electron.* **2014**, *29*, 4288–4300. [CrossRef]
3. Liu, J.; Liu, Z. Harmonic Analyzing of the Double PWM Converter in DFIG Based on Mathematical Model. *Energies* **2017**, *10*, 2087. [CrossRef]
4. Liu, Y.; Xu, J.; Shuai, Z.; Li, Y.; Peng, Y.; Liang, C.; Cui, G.; Hu, S.; Zhang, M.; Xie, B. A Novel Harmonic Suppression Traction Transformer with Integrated Filtering Inductors for Railway Systems. *Energies* **2020**, *13*, 473. [CrossRef]
5. Raizer, A.; Silva, J.V.D.; Fonseca, M.P. Analysis of harmonic current emissions in voltages below the presented by the Standard IEC 61000-3-2. In Proceedings of the 2017 IEEE 3rd Global Electromagnetic Compatibility Conference (GEMCCON), Sao Paulo, Brazil, 8–10 November 2017; pp. 1–4.
6. Cao, K.; Liu, X.; He, M.; Meng, X.; Zhou, Q. Active-Clamp Resonant Power Factor Correction Converter With Output Ripple Suppression. *IEEE Access* **2021**, *9*, 5260–5272. [CrossRef]
7. Li, H.; Li, S.; Xiao, W. Single-Phase LED Driver With Reduced Power Processing and Power Decoupling. *IEEE Trans. Power Electron.* **2021**, *36*, 4540–4548. [CrossRef]
8. Huynh, P.S.; Ronanki, D.; Vincent, D.; Williamson, S.S. Direct AC–AC Active-Clamped Half-Bridge Converter for Inductive Charging Applications. *IEEE Trans. Power Electron.* **2021**, *36*, 1356–1365. [CrossRef]
9. Wang, Y.; Deng, X.; Wang, Y.; Xu, D. Single-Stage Bridgeless LED Driver Based on a CLCL Resonant Converter. *IEEE Trans. Ind. Appl.* **2018**, *54*, 1832–1841. [CrossRef]
10. Ali, K.; Dube, S.K.; Das, P.; Peng, J.C.; Rogers, D.J. Improvement of ZVS Range and Current Quality of the Nine-Switch Single-Stage AC–DC Converter. *IEEE Trans. Power Electron.* **2020**, *35*, 4658–4668. [CrossRef]
11. Alayi, R.; Zishan, F.; Mohkam, M.; Hoseinzadeh, S. A Sustainable Energy Distribution Configuration for Microgrids Integrated to the National Grid Using Back-to-Back Converters in a Renewable Power System. *Electronics* **2021**, *10*, 1826. [CrossRef]
12. Hoseinzadeh, S.; Ghasemi, M.H.; Heyns, S. Application of hybrid systems in solution of low power generation at hot seasons for micro hydro systems. *Renew. Energy* **2020**, *160*, 323–332. [CrossRef]
13. Narimani, M.; Moschopoulos, G. A New Interleaved Three-Phase Single-Stage PFC AC–DC Converter. *IEEE Trans. Ind. Electron.* **2014**, *61*, 648–654. [CrossRef]
14. Alonso, J.M.; Dalla Costa, M.A.; Ordiz, C. Integrated Buck-Flyback Converter as a High-Power-Factor Off-Line Power Supply. *IEEE Trans. Ind. Electron.* **2008**, *55*, 1090–1100. [CrossRef]
15. Mishima, T.; Sakamoto, S.; Ide, C. ZVS Phase-Shift PWM-Controlled Single-Stage Boost Full-Bridge AC–AC Converter for High-Frequency Induction Heating Applications. *IEEE Trans. Ind. Electron.* **2017**, *64*, 2054–2061. [CrossRef]
16. Kim, J.; Choi, H.; Won, C. New Modulated Carrier Controlled PFC Boost Converter. *IEEE Trans. Power Electron.* **2018**, *33*, 4772–4782. [CrossRef]
17. Xu, H.; Chen, D.; Xue, F.; Li, X. Optimal Design Method of Interleaved Boost PFC for Improving Efficiency from Switching Frequency, Boost Inductor, and Output Voltage. *IEEE Trans. Power Electron.* **2019**, *34*, 6088–6107. [CrossRef]
18. Narimani, M.; Moschopoulos, G. Analysis and design of a new three-level PFC AC-DC converter. In Proceedings of the 2013 IEEE Energy Conversion Congress and Exposition, Denver, CO, USA, 15–19 September 2013; pp. 4808–4813.
19. Lee, S.; Do, H. Soft-Switching Two-Switch Resonant AC–DC Converter With High Power Factor. *IEEE Trans. Ind. Electron.* **2016**, *63*, 2083–2091. [CrossRef]

20. Golbon, N.; Moschopoulos, G. A Low-Power AC–DC Single-Stage Converter With Reduced DC Bus Voltage Variation. *IEEE Trans. Power Electron.* **2012**, *27*, 3714–3724. [CrossRef]
21. Luo, Q.; Ma, K.; He, Q.; Zou, C.; Zhou, L. A Single-Stage High-Frequency Resonant AC/AC Converter. *IEEE Trans. Power Electron.* **2017**, *32*, 2155–2166. [CrossRef]
22. Luo, Q.; Zhi, S.; Zou, C.; Lu, W.; Zhou, L. An LED Driver With Dynamic High-Frequency Sinusoidal Bus Voltage Regulation for Multistring Applications. *IEEE Trans. Power Electron.* **2014**, *29*, 491–500. [CrossRef]
23. Lee, M.; Lai, J.-S. Spread-Spectrum Frequency Modulation With Adaptive Three-Level Current Scheme to Improve EMI and Efficiency of Three-Level Boost DCM PFC. *IEEE Trans. Power Electron.* **2021**, *36*, 2476–2480. [CrossRef]
24. Lee, M.; Lai, J.-S. Unified Voltage Balancing Feedforward for Three-Level Boost PFC Converter in Discontinuous and Critical Conduction Modes. *IEEE Trans. Circuits Syst. II Exp. Briefs* **2021**, *68*, 441–445. [CrossRef]
25. Yao, K.; Hu, W.; Li, Q.; Lyu, J. A Novel Control Scheme of DCM Boost PFC Converter. *IEEE Trans. Power Electron.* **2015**, *30*, 5605–5615. [CrossRef]
26. Xiang, Z.; Pang, Y.; Wang, L.; Wong, C.; Lam, C.; Wong, M. Design, control and comparative analysis of an LCLC coupling hybrid active power filter. *IET Power Electron.* **2020**, *13*, 1207–1217. [CrossRef]
27. Shafiei, N.; Pahlevaninezhad, M.; Farzanehfard, H.; Motahari, S.R. Analysis and Implementation of a Fixed-Frequency LCLC Resonant Converter With Capacitive Output Filter. *IEEE Trans. Ind. Electron.* **2011**, *58*, 4773–4782. [CrossRef]
28. Lin, R.; Huang, L. Efficiency Improvement on LLC Resonant Converter Using Integrated LCLC Resonant Transformer. *IEEE Trans. Ind. Appl.* **2018**, *54*, 1756–1764. [CrossRef]
29. Pini, S.; Barbi, I. A single-phase high-power-factor rectifier, based on a two-quadrant shunt active filter. *IEEE Trans. Power Electron.* **2011**, *26*, 3131–3143. [CrossRef]
30. Senturk, O.S.; Hava, A.M. Performance enhancement of the single-phase series active filter by employing the load voltage waveform reconstruction and line current sampling delay reduction methods. *IEEE Trans. Power Electron.* **2011**, *26*, 2210–2220. [CrossRef]
31. Tang, Y.; Loh, P.; Wang, P.; Choo, F.; Gao, F. Exploring inherent damping characteristic of LCL-filters for three-phase grid-connected voltage source inverters. *IEEE Trans. Power Electron.* **2012**, *27*, 1433–1443. [CrossRef]
32. Iftikhar, M.U.; Sadarnac, D.; Karimi, C. Input filter damping design for control loop stability of DC–DC converters. In Proceedings of the 2007 IEEE International Symposium on Industrial Electronics, Vigo, Spain, 4–7 June 2007; pp. 353–358.
33. Yu, X.; Salato, M. An Optimal Minimum-Component DC–DC Converter Input Filter Design and Its Stability Analysis. *IEEE Trans. Power Electron.* **2014**, *29*, 829–840.
34. Guo, W.; Jain, P.K. A low frequency AC to high frequency AC inverter with build-in power factor correction and soft-switching. *IEEE Trans. Power Electron.* **2004**, *19*, 430–442. [CrossRef]
35. Liserre, M.; Blaabjerg, F.; Hansen, S. Design and control of an LCL-filter-based three-phase active rectifier. *IEEE Trans. Ind. Appl.* **2005**, *41*, 1281–1291. [CrossRef]
36. Jalili, K.; Bernet, S. Design of LCL Filters of Active-Front-End Two-Level Voltage-Source Converters. *IEEE Trans. Ind. Electron.* **2009**, *56*, 1674–1689. [CrossRef]
37. Basu, K.; Sahoo, A.K.; Chandrasekaran, V.; Mohan, N. Grid-Side AC Line Filter Design of a Current Source Rectifier With Analytical Estimation of Input Current Ripple. *IEEE Trans. Power Electron.* **2014**, *29*, 6394–6405. [CrossRef]
38. Athab, H.S.; Lu, D.D. A High-Efficiency AC/DC Converter With Quasi-Active Power Factor Correction. *IEEE Trans. Power Electron.* **2010**, *25*, 1103–1109. [CrossRef]
39. Sahoo, A.K.; Basu, K.; Mohan, N. Systematic Input Filter Design of Matrix Converter by Analytical Estimation of RMS Current Ripple. *IEEE Trans. Ind. Electron.* **2015**, *62*, 132–143. [CrossRef]
40. *ENERGY STAR: Program Requirements for Solid State Lighting Luminaires*; Environmental Protection Agency and U.S. Department of Energy: Washington, DC, USA, 2008. Available online: https://www.osti.gov/biblio/1218258-energy-star-program-requirements-solid-state-lighting-luminaires (accessed on 1 November 2021).
41. Lloyd, H. *Dixon, Unitrode Magnetics Design Handbook*; Texas Instruments: Dallas, TX, USA, 2001.